



HAL
open science

Quantifying frozen melt in crustal rocks: A new melt-o-meter based on zircon rim volumes

M. Mintrone, A. Galli, Oscar Laurent, C. Chelle-Michou, M.W. Schmidt

► To cite this version:

M. Mintrone, A. Galli, Oscar Laurent, C. Chelle-Michou, M.W. Schmidt. Quantifying frozen melt in crustal rocks: A new melt-o-meter based on zircon rim volumes. *Chemical Geology*, 2020, 551, pp.119755. 10.1016/j.chemgeo.2020.119755 . hal-02934816

HAL Id: hal-02934816

<https://hal.science/hal-02934816>

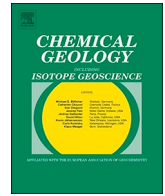
Submitted on 10 Sep 2020

HAL is a multi-disciplinary open access archive for the deposit and dissemination of scientific research documents, whether they are published or not. The documents may come from teaching and research institutions in France or abroad, or from public or private research centers.

L'archive ouverte pluridisciplinaire **HAL**, est destinée au dépôt et à la diffusion de documents scientifiques de niveau recherche, publiés ou non, émanant des établissements d'enseignement et de recherche français ou étrangers, des laboratoires publics ou privés.



Distributed under a Creative Commons Attribution - NoDerivatives 4.0 International License



Quantifying frozen melt in crustal rocks: A new melt-o-meter based on zircon rim volumes

M. Mintrone^{a,*}, A. Galli^a, O. Laurent^{a,b}, C. Chelle-Michou^a, M.W. Schmidt^a

^a Department of Earth Sciences, ETH Zurich, Sonneggstrasse 5, 8092 Zurich, Switzerland

^b CNRS, Geosciences Environnement Toulouse, UMR5563-CNRS-CNES-IRD-UPS, Observatoire Midi-Pyrénées, 14 avenue Edouard Belin, F-31400 Toulouse, France

ARTICLE INFO

Editor: Donald Dingwell

Keywords:

Zircon

Melt fraction

Migmatites

Crustal anatexis

ABSTRACT

Quantifying the distribution of granitic melt at all scales in mid- to lower crustal migmatitic terranes is critical to understand crustal melting processes, chemical differentiation of the crust and its rheological behavior during deformation. We propose a new method to determine the fraction of frozen granitic melt on a hand specimen scale based on the relative volumes of newly precipitated to total zircon (FPZ = Fraction of newly Precipitated Zircon) as obtained by image analysis on dated zircon cores and rims. Using the calculated Zr-solubility $[Zr]^{sat}$ in the melt at the inferred melting temperature and the Zr concentration in the bulk sample $[Zr]^{bulk}$, the fraction of melt F_{melt} can be determined through $F_{melt} = FPZ \times [Zr]^{bulk} / [Zr]^{sat}$. The such obtained F_{melt} corresponds to the melt fraction in the hand specimen at the time the system closed for melt mobility. Thermodynamic modelling further allows estimation of H₂O-contents required to maintain the melt fraction obtained from the melt-o-meter in a molten stage. The applicability of this method has been tested on eight migmatitic samples with peak temperatures between 725 and 925 °C. Most of the lower temperature migmatites (<750 °C) retained F_{melt} of 0.15–0.25 (± 0.03 –0.05), a melt fraction below or at the static melt escape threshold. In contrast, most of the higher-temperature migmatites (>800 °C) retained F_{melt} of 0.35–0.50 (± 0.07 –0.10). At these melt fractions, melt extraction and melt migration from and within the source should be efficient. Consequently, these samples are likely open-system migmatites affected by melt accumulation or depletion processes. The melt-o-meter requires that the rock types under consideration produced a granitic melt that remained zircon-saturated and is therefore restricted to migmatitic meta-sediments and meta-granitoids. When applied carefully, this melt-o-meter offers a new and powerful tool to not only quantify melt distribution but also evaluate the extent of melt mobility in migmatites.

1. Introduction

Crustal melting and related magmatic weakening are key factors controlling the thermo-mechanical behavior of crustal rocks (Labrousse et al., 2015). In fact, with melt fraction reaching 7–10 vol% (the melt connectivity threshold, Rosenberg and Handy, 2005), rock strength dramatically drops by 90%. In addition, deformation-enhanced melt segregation (Rutter and Neumann, 1995; Holtzman et al., 2003), extraction and accumulation control melt flow through the crust and in turn, crustal differentiation (Sawyer, 1994). Therefore, quantifying the amount of melt in crustal rocks and melt distribution on a larger scale is crucial to deciphering the rheological and compositional architecture of migmatitic terranes and their response to deformation (e.g. Vanderhaeghe, 2009). Unfortunately, the accurate quantification of the amount of melt in migmatites remains difficult. In this context, visual

estimates of the fraction of leucosome present in an outcrop is futile as leucosomes are not equal to melt but represent crystal mushes constituted by liquid and solid phases (residual and peritectic) or melt-infiltrated or melt-fractionated domains (Sawyer, 1987, 2008; Brown et al., 1995; Stevens et al., 2007).

Commonly, the quantification of melt fraction in migmatites relies on thermodynamic modelling and is based on pseudosections contoured for vol% of melt (e.g. White et al., 2001). Two intrinsic limitations irremediably affect such melt estimates: first, melt fractions strongly depend on bulk H₂O at the time of melting, a parameter that is not conserved and cannot be determined directly. This dependence on H₂O-content becomes increasingly important as the bulk rock composition approaches that of eutectic granite. Secondly, melt has to be stepwise re-integrated into the residual composition to retrieve the fertile source rock composition before melting (White et al., 2004). This is

* Corresponding author.

E-mail address: michael.mintrone@erdw.ethz.ch (M. Mintrone).

<https://doi.org/10.1016/j.chemgeo.2020.119755>

Received 27 March 2020; Received in revised form 2 June 2020; Accepted 13 June 2020

Available online 17 June 2020

0009-2541/ © 2020 The Authors. Published by Elsevier B.V. This is an open access article under the CC BY-NC-ND license

(<http://creativecommons.org/licenses/by-nc-nd/4.0/>).

particularly challenging in granulites at temperatures above the biotite-dehydration melting (e.g. Bartoli, 2017), where large amounts of melt may have been lost (White et al., 2004; Mayne et al., 2016).

The amount of melt calculated in pseudosections of a given bulk composition corresponds to the quantity of melt at pressure, temperature and an estimated H₂O-content. This melt fraction does not necessarily coincide with the amount of melt ever formed, ever transited or finally preserved in this rock. De facto, melt segregation, extraction, migration, depletion and accumulation are efficient mechanisms to redistribute melt at all scales through the crust (Sawyer, 1994). Melt in- and out-fluxes from micro- to macro-scales are not quantifiable with thermodynamic modelling alone.

During crustal melting, accessory zircon is partly or totally dissolved into the melt, the solubility $[Zr]^{sat}$ depending on temperature and melt composition as described by zircon saturation equations (Watson and Harrison, 1983; Boehnke et al., 2013). Complete zircon dissolution is rarely reached, as testified for by abundant inherited zircon cores in crust-derived granites (Villars et al., 2009), in residual granulites (Villaseca et al., 2011) and by multiple age domains in zircons from high-grade poly-metamorphic rocks (Gerdes and Zeh, 2009). Mass balance dictates that besides $[Zr]^{sat}$, the extent of zircon preservation during melting depends on the zircon content of the source rock and on melt fraction (Kelsey et al., 2008; Watson, 1996). Surprisingly, the influence of these parameters has not been fully explored yet, although this potentially offers a powerful tool to relate zircon dissolution/precipitation during anatexis to melt fraction present in a given rock volume at the time of zircon crystallization.

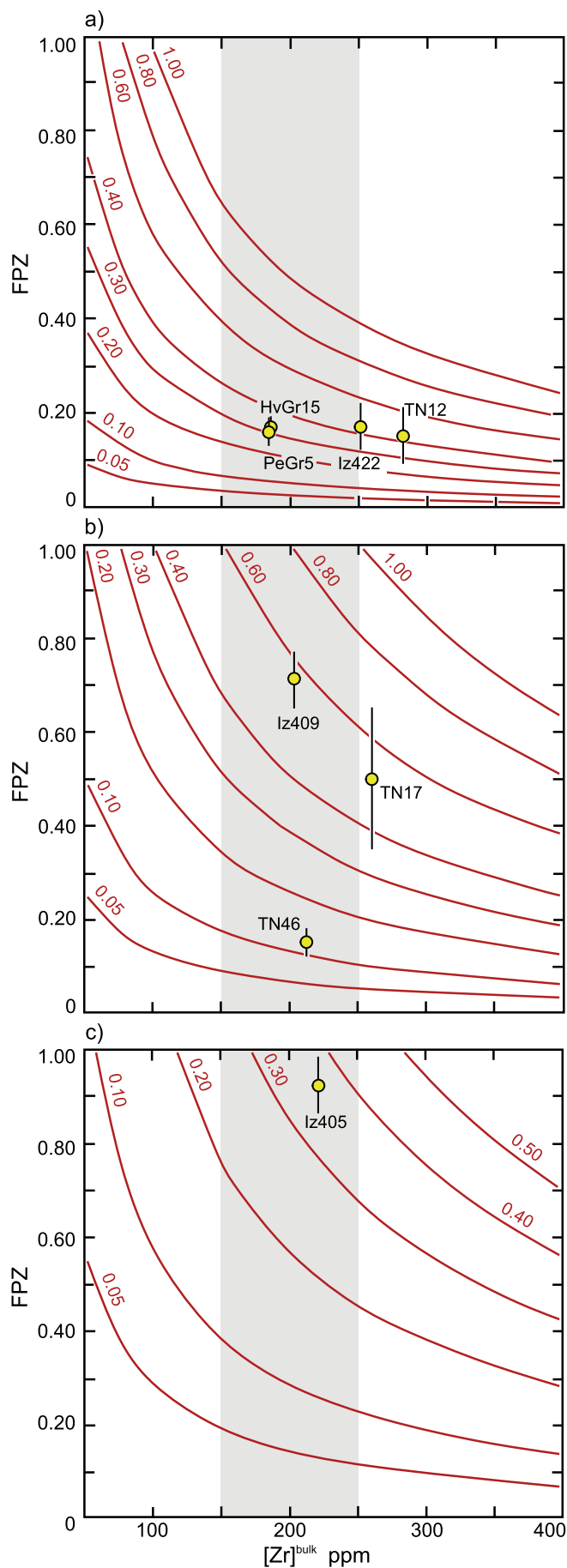
In this study, we propose a melt-o-meter that provides the amount of melt present in the rock when zircon rims crystallized from the melt. Our approach does not inform on rock fertility but quantifies the fraction of melt at the time the system closed for melt mobility, being therefore complementary to pseudosections. The fundamental data required are obtained through zircon grain image analysis and a statistical treatment thereof, and by U–Pb dating of zircon cores and rims. The zircon-rim-volume melt-o-meter is applied on eight samples from three well-documented migmatite terranes at various P-T conditions and rock compositions. We further discuss closed vs. open system behavior, fluid-fluxed vs. fluid-absent melting and implications for the rheology of migmatitic rocks.

2. A new melt-o-meter based on zircon rim volumes

2.1. FPZ – fraction of (newly) precipitated zircon

Most of the major minerals involved in melting reactions of crustal felsic rocks at temperatures < 900 °C, i.e. feldspars, quartz and micas, have negligible Zr concentrations of < 10 ppm (Bea et al., 2006). Only garnet and amphibole can potentially incorporate larger amount of Zr, even so only < 80 ppm at $T < 900$ °C (Kohn et al., 2015). Among the accessory phases, zircon has orders of magnitude more Zr (ca. 500,000 ppm) than titanite, ilmenite and rutile (max. 600–5000 ppm) or monazite and apatite (< 15 ppm, Bea et al., 2006). Thus, at supra-solidus conditions < 900 °C, the bulk of the Zr budget in meta-sedimentary and -granitic rocks is partitioned between residual zircon and melt. Likewise, the budget of Zr dissolved in anatectic melts essentially relates to zircon dissolution.

During prograde melting, quartzo-feldspathic melts dissolve tens to hundreds of ppm Zr, which, for a given temperature and melt composition, may be calculated as Zr saturation concentration $[Zr]^{sat}$ following Watson and Harrison (1983) and Boehnke et al. (2013). The partial or complete dissolution of zircon is much faster than the duration of crustal melting events (10^3 – 10^4 years vs $> 10^6$ years, respectively, Harrison and Watson, 1983; Harris et al., 2000; Kelsey et al., 2008; Villars et al., 2009), rendering prograde zircon dissolution likely an equilibrium process. In a partially molten zircon saturated rock, one may express the mass fraction of zircon precipitated from this melt, i.e.



(caption on next page)

Fig. 1. Plots of the Fraction of newly Precipitated Zircon (FPZ) as a function of bulk rock Zr-concentration, calculated for different fractions of melt (red curves) using Eq. (2). The gray area indicates the characteristic $[Zr]^{bulk}$ of (meta-) granitoids and metapelites. The yellow symbols represent the samples used for testing of the melt-o-meter, error bars are 2σ . Note that the isopleths are for 700, 800, and 900 °C and a M value of 1.3 (corresponding to an average eutectic granite melt), samples are simply plotted in the diagram of the nearest temperature value. (For interpretation of the references to colour in this figure legend, the reader is referred to the web version of this article.)

a zircon rim formed upon cooling and/or decompression (Kelsey et al., 2008), relative to total zircon (preserved core + new rim) as “fraction of precipitated zircon”.

$$FPZ = \frac{V_{zircon}^{rim}}{V_{zircon}^{rim} + V_{zircon}^{core}} \quad (1)$$

where V_{zircon}^{rim} and V_{zircon}^{core} are the volumes of zircon rims and cores in the sample. Below, we propose a method to estimate these volumes based on cathodoluminescence (CL) images.

Simple mass balance relates FPZ to the melt fraction F_{melt} , Zr-solubility and bulk Zr concentration $[Zr]^{bulk}$ (see Supplementary Data):

$$FPZ = F_{melt} \times [Zr]^{sat} / [Zr]^{bulk} \quad (2)$$

Zr solubility with respect to zircon is given by $[Zr]^{sat} = \frac{500000}{\exp\left(\left(\frac{10108}{T}\right) - 1.16 \times (M - 1) - 1.48\right)}$ in ppm (Boehnke et al., 2013), where T is temperature in K and M a molar melt composition parameter based on the cation fraction $(Na + K + 2 \times Ca) / (Al \times Si)$. At a given temperature and melt composition, FPZ therefore only depends on $[Zr]^{bulk}$ and F_{melt} (Fig. 1). F_{melt} can then be calculated as (Fig. 1):

$$F_{melt} = FPZ \times [Zr]^{bulk} / [Zr]^{sat} \quad (3)$$

Note that in quartzo-feldspathic rocks, F_{melt} is mainly controlled by the availability of fluid. However, H_2O itself does not control Zr-solubility in granitic melts and is not included in the melt compositional parameter M, so that knowing H_2O -concentrations is not required to use Eq. (3).

2.2. Effect of temperature, melt composition and $[Zr]^{bulk}$ on FPZ

Implicit to the zircon saturation models, the primary parameter controlling zircon dissolution is temperature. At constant M, $[Zr]^{bulk}$ and F_{melt} , Zr-solubility and hence the FPZ increases with increasing temperature (Fig. 1). Of course, in any closed system, F_{melt} increases

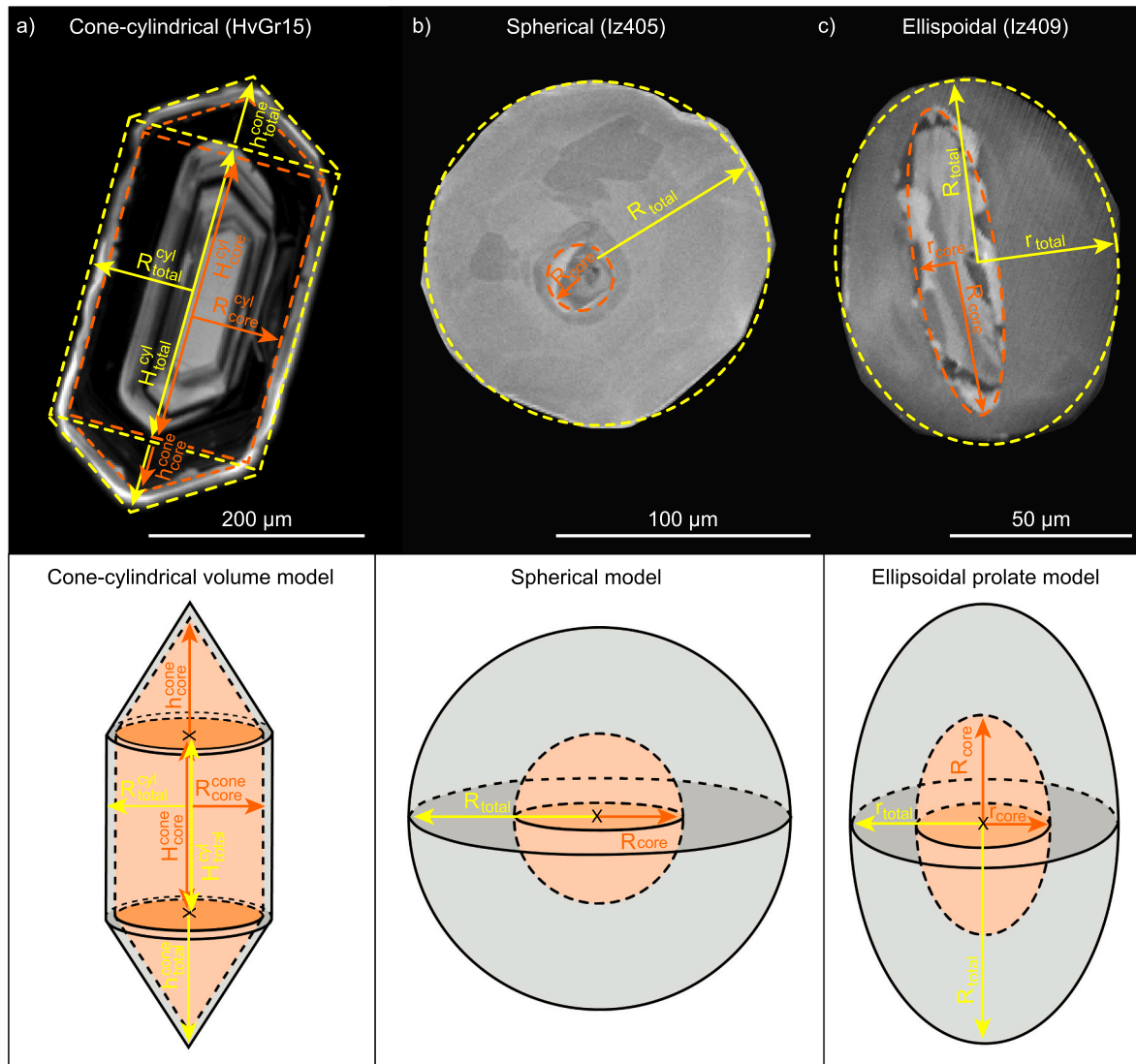


Fig. 2. Schematic illustration of the geometrical approximations applied to calculate zircon rim volumes for three different, end-member zircon geometries, i.e. 2 cones + cylindrical (a); spherical (b) and prolate ellipsoidal (c), with corresponding 3D rotational models.

with temperature further enhancing the effect of temperature. The M values of most crustal melts derived from meta-sedimentary or meta-igneous sources fall in a rather restricted range (at most M from 1.1–1.4) as melts are close to the granitic minimum, yielding a maximum inaccuracy on $[\text{Zr}]^{\text{sat}}$ of $\pm 10\%$ relative (see Supplementary Data, Fig. S1).

On the other hand, at constant temperature and M (i.e., given $[\text{Zr}]^{\text{sat}}$), the fraction of dissolved zircon, which is equal to the FPZ in a closed system, is inversely proportional to $[\text{Zr}]^{\text{bulk}}$ and directly proportional to F_{melt} (Eq. (2)). For a $[\text{Zr}]^{\text{bulk}}$ of 150–250 ppm, as characteristic for most crustal rocks (Rudnick and Gao, 2003), a melt fraction of 1.00 leads to a maximum dissolved zircon fraction of 0.65 of zircon at 700 °C (Fig. 1a), whereas all zircon dissolves completely at melt fractions of 0.60–1.00 at 800 °C and at melt fractions of 0.25–0.45 at 900 °C (Fig. 1b, c).

2.3. Estimating zircon rim volumes in migmatites

For each single zircon crystal, the volume of zircon rim ($V_{\text{zircon}}^{\text{rim}}$) is calculated as the difference between the total zircon volume ($V_{\text{zircon}}^{\text{total}}$) and the volume of zircon core ($V_{\text{zircon}}^{\text{core}}$). The latter are obtained by measuring the length, width or radius of each crystal in 2D longitudinal main sections in cathodoluminescence (CL, Fig. 2). As will be discussed below, it is crucial for the 2D/3D conversion to mount well sorted grain sizes in order to approximate best the longitudinal main section, i.e. the section containing the 4-fold symmetry axis. Depending on the grain, the outer zircon shape and the zircon core shape are approximated either as ideal spheres or prolate rotational ellipsoids or as a combination of a cylinder and two cones (Fig. 2a, b, c), the rotational axis of these bodies always being identical with the zircon c-axis. The cathodoluminescence-distinction between newly formed zircon rim and preserved zircon core has to be confirmed by spatially resolved (LA-ICP-MS or SIMS) U–Pb dating. To obtain a true average and to enable a meaningful statistical analysis, all measurable zircons have to be considered, even if no rim or core are visible. The uncertainty in the rim volume estimate depends upon how accurately the core/rim volume ratio is described by the geometrical approximation used. In principle, geometrically simple, intact zircon grains polished to their longitudinal main section should be used to minimize inaccuracy and uncertainty. Nevertheless, it is strongly recommended that a sufficiently large zircon population is taken into account (see Figs. 4, 7 and Section 4 for details).

3. Application of the melt-o-meter to natural migmatites

3.1. Tested samples

Our melt-o-meter is applied to eight well-documented migmatitic samples spanning a broad range of crustal melting conditions and bulk rock compositions (Table 1). Samples HvGr15 and PeGr5 are migmatitic orthogneisses from the Gruf Complex in the European Central Alps, characterized by Oligocene melting conditions of 700–750 °C and 7 kbar (Galli et al., 2012, 2013). Both samples are homogeneous at the hand specimen scale, slightly foliated and mostly composed of quartz, plagioclase, alkali feldspar and biotite (10–15%). Samples TN46 and TN17 are migmatitic paragneisses formed at 750–850 °C and 4.5 kbar (Barbey et al., 2015) in the Carboniferous Velay Complex of the French Massif Central. TN46 is mainly composed of quartz, plagioclase, alkali-feldspar, biotite (10–20%), TN17 is mainly made of centimetric quartz-, plagioclase- and alkali-feldspar-rich leucosome bands alternating with biotite-rich melanosome bands and fine- to medium-grained mesosome bands (Chelle-Michou et al., 2017). Sample TN12 is a banded migmatitic orthogneiss from the same area. It is constituted by alternating leucocratic bands rich in quartz, plagioclase and alkali-feldspar and more melanocratic, biotite-rich bands equilibrated at 750 °C and 9 kbar (Gardien et al., 1997).

Samples Iz422, Iz409 and Iz405 are migmatitic metapelites from the Ivrea Zone in the European Southern Alps formed in Permian time. They crystallized along a P-T gradient, with melting conditions of 750 °C and 6 kbar; 825 °C and 8 kbar; and 925 °C and 9 kbar, respectively (Redler et al., 2013; Kunz et al., 2018). The three samples are made of quartz, plagioclase, alkali-feldspar, sillimanite, biotite and garnet. With increasing temperature, the amounts of garnet and rutile increase while that of biotite decreases.

3.2. Zircon morphology and estimated FPZ and corresponding F_{melt}

Representative CL images of zircon crystals from these samples are presented in Fig. 3. Zircons from the two samples of the Gruf Complex (HvGr15 and PeGr5) occur as homogenous elongated and prismatic grains, with a grain size varying between 200 and 600 μm in length and 100 and 200 μm in width (Fig. 3a, b). They display oscillatory zoned Permian cores, generally surrounded and truncated by bright and homogenous Oligocene rims, interpreted as the result of partial melting (Galli et al., 2012). In both samples, the calculated rim volume fractions show a Gaussian distribution (Fig. 4a, b) ranging mostly between 0 and 0.30, corresponding to average FPZs of 0.17 and 0.16, respectively (Table 1).

Zircons from the three samples of the French Massif Central (TN12, TN46 and TN17) are prismatic to rounded in shape. Their grain sizes vary between 100 and 400 μm in length and 100 to 200 μm in width. These zircons have planar and oscillatory zoned cores, which are Neoproterozoic in TN46 and TN17 (Fig. 3e, f) but Ordovician in TN12 (Fig. 3d) (Chelle-Michou et al., 2017). Cores are surrounded and truncated by dark rims of Carboniferous age, interpreted to be formed as result of partial melting (Fig. 3d, e, f) (Chelle-Michou et al., 2017). Calculated rim volume fractions in samples TN12 and TN46 range between 0 and 0.50, with a non-homogenous distribution for TN12 (Fig. 4d) and a Gaussian distribution for TN46 (Fig. 4e), both samples yielding an FPZ of 0.15 (Table 1). Sample TN17 is characterized by strongly heterogeneous rim volume fractions (Fig. 4f). Three zircon populations occur: one with no visible rims, one with fully neofomed grains and one characterized by zircon with clearly discernable rim/core relationship, but variable rim proportions. The average FPZ is 0.50 (Table 1).

Zircon from the three samples of the Ivrea Zone (Iz422, Iz409 and Iz405) is mainly sub-euhedral and rounded, even spherical in Iz409 and Iz405. Grain sizes range between 50 and 300 μm in length and 30 to 150 μm in width. Sample Iz422 and Iz409 show oscillatory to sector zoned, bright Ordovician to Precambrian cores, surrounded by thin, inclusion-rich, bright rims attributed to fluid-induced (re-)crystallization (Kunz et al., 2018; Fig. 3c). The cores and the bright rims are further surrounded and truncated by homogenous or slightly oscillatory zoned, dark rims of Permian age, crystallized during partial melting (Kunz et al., 2018, Fig. 3c, g). In contrast, zircons in sample Iz405 are bright, oscillatory zoned or exhibit rare cores surrounded by thick, bright oscillatory to sector zoned rims (Fig. 3h). The bright, oscillatory to sector zoned domains are Permian in age and related to partial melting (Kunz et al., 2018). In sample Iz422, zircon grains have a rim volume fraction of 0 to 0.80, but most of the measurements are within 0–0.20 (Fig. 4c), this sample yields an FPZ of 0.17 (Table 1). Zircons in sample Iz409 display a clear bi-modal population of rim volume fraction (Fig. 4g), with modes at around 0.20 and >0.90, yielding an average FPZ of 0.72. Zircon grains in sample Iz405 have a Gaussian rim volume distribution of 0.90–1.00 (Fig. 4h), corresponding to an average FPZ of 0.92 (Table 1).

We have applied our melt-o-meter on all test samples, using for each sample the published $[\text{Zr}]^{\text{bulk}}$, the inferred melting temperature, and the M parameter corresponding to melt composition obtained from thermodynamic modelling for each sample at their peak temperature conditions (Table 1). Two samples at 725 °C (HvGr15, PeGr5) yield $F_{\text{melt}} = 0.23$ and 0.21, two samples at 750 °C (TN12 and Iz422) yields

Table 1
Summary of the studied samples and parameters used for calculation.

Samples			Melt-o-meter					Thermodynamic modelling (literature)	
Name	Location	Rock types	T°C	M	[Zr] ^{bulk} ppm	N*	FPZ	F _{melt}	F _{melt} ^{pseudosection}
HvGr15	Gruf	Og	725	1.4	186	30	0.17(2)	0.23(3)	0.10–0.30 ^a
PeGr5	Gruf	Og	725	1.4	185	42	0.16(3)	0.21(4)	
Iz422	Ivrea	Mp	750	1.3	255	49	0.17(5)	0.27(8)	0.05–0.15 ^c
TN12	M. Central	Og	750	1.4	283	29	0.15(6)	0.24(10)	0.05–0.25 ^b
TN46	M. Central	Mp	800	1.3	213	45	0.15(3)	0.13(3)	0.15–0.40 ^b
TN17	M. Central	Mp	800	1.3	261	27	0.50(15)	0.52(16)	
Iz409	Ivrea	Mp	825	1.3	204	127	0.72(6)	0.47(4)	0.10–0.30 ^c
Iz405	Ivrea	Mp	925	1.2	220	35	0.92(6)	0.34(2)	0.30–0.50 ^c

N* correspond to the number of zircons measured to calculate FPZ (= Fraction of newly Precipitated Zircon). Og and Mp correspond to orthogneiss and metapelite respectively.

^a Estimated melt fraction from Galli et al., 2012.

^b Estimated melt fraction from Barbey et al., 2015.

^c Estimated melt fraction from Redler et al., 2013. The digits between brackets in the FPZ and F_{melt} columns correspond to the uncertainty on the last significant digit(s). Note that uncertainty on F_{melt} are a minimum, as they only correspond to the relative uncertainty on FPZ.

F_{melt} = 0.24 and 0.27, two samples at 800 °C (TN46 and TN17) give F_{melt} = 0.13 and 0.52, one sample at 825 °C (Iz409) yields F_{melt} = 0.47, and one sample at 925 °C (Iz405) gives F_{melt} = 0.34 (Table 1).

3.3. H₂O content obtained by thermodynamic modelling

At a given temperature, pressure and bulk composition, the obtained F_{melt} using the melt-o-meter corresponds to a certain bulk H₂O content. This amount of bulk H₂O is required to maintain the melt in a liquid state at the given conditions.

Assuming a closed system (except for H₂O), F_{melt} obtained from our melt-o-meter can therefore be combined with thermodynamic modelling to determine bulk and melt H₂O-contents at these conditions. For this purpose, we calculated T-X_{H₂O} pseudosections which quantify F_{melt} as a function of H₂O-content (Fig. S3). These pseudosections were calculated in the NaCaKFMASiOH system using Perple_X (Connolly, 2005), the dataset of Holland and Powell (2011) and mineral solution models listed in the supplementary data. Calculations were performed for 650–950 °C and 0.1–4 wt% bulk H₂O, covering most melting conditions reported for continental crust (Weinberg and Hasalová, 2015). For each sample, melt fraction (F_{melt}) and composition (M) were retrieved each 10 °C along isobaric temperature paths calculated for H₂O intervals of 0.5 wt%. F_{melt} and M were then used to calculate [Zr]^{sat} (Boehnke et al., 2013) and FPZ from Eq. (2). Using the measured FPZ at a given temperature, H₂O concentrations in the melt and bulk can thus be determined from the isopleth of bulk H₂O, necessary to maintain the calculated amount of melt in a liquid state (Fig. 5).

For samples HvGr15 and PeGr5 formed at 725 °C and TN12 and Iz422 formed at 750 °C, calculated bulk H₂O contents are 2.2–3.5 wt% (Fig. 5a–d). This amount of H₂O corresponds to the H₂O soluble in the melt at F_{melt} = 0.21–0.27, and to some minor H₂O in biotite. Samples TN46, TN17 and Iz409 crystallized at 800–825 °C display variable F_{melt} of 0.13–0.52, which yields bulk H₂O contents of 0.9–3 wt% (Fig. 5e–g). Sample Iz405, which experienced temperatures of 925 °C, yields ~1.4 wt% bulk H₂O at F_{melt} = 0.34 (Fig. 5h). Note that these H₂O-contents have uncertainties in the order of 1 wt%-absolute (Fig. 5).

4. Discussion of rim fraction determination and resulting melt fraction

4.1. Robustness of zircon rim fractions

The analysis of zircon rim volume fractions is not necessarily straightforward. Besides essential geometrical considerations, critical issues are a selectiveness on grain size when preparing mounts that leads to a non-representative zircon population, a grain size

dependence of rim fraction, and bimodal or more complex zircon rim volume distributions.

Any deviation from the longitudinal main section affects calculated rim fractions (FPZ). However, if zircons are exposed within 10% (with respect to the grain radius) of their 4-fold symmetry axis, FPZ is correctly estimated within a percent of relative rim volumes. At 20 and 30% from the 4-fold symmetry axis, variations are within 3 and 8%, respectively (see Supplementary Data, Fig. S2). A systematic deviation from the main section will lead to an overestimation of rim fractions, underlining the importance of a meticulous size sorted mount preparation.

Secondly, older and in particular corroded zircon cores may not be centered with respect to the newly grown outer crystal shape, such that if the main section does not cut the core center, rim fractions of individual grains can then be both over- and underestimated (Fig. S2). As a net-effect, irregular growth rims broaden the statistical rim fraction (FPZ) distribution, i.e. increase the standard deviation. This underlines the necessity of analyzing a sufficient number of zircons to obtain a well constrained statistical FPZ-distribution.

Thirdly, in many samples zircon grains < 20 µm are more common than larger ones, yet, for good reasons the larger grains are generally selected for mounting and dating. Kawakami et al. (2013), investigating the zircon size distribution in migmatitic metapelites, found a log-linear grain size distribution cumulating at ~80 µm. Although the size fraction < 20 µm contained ~80% of the grains, this amounts to only 12% of the total zircon volume proportions. Hence, focusing on the more measurable grains > 20 µm does not strongly bias rim volume proportions (Fig. 6a). Nevertheless, Ostwald ripening, i.e. the preferential dissolution of small grains and preferential precipitation on or of larger grains (Nemchin et al., 2001), may lead to a grain size dependence of rim fractions. To test this effect, we investigated a sample with a heterogeneous size distribution (Iz409). As shown in Fig. 6b, rim volume fractions of each size category corresponds within uncertainty to the average rim fraction (FPZ) determined from the whole population (0.72 ± 0.06). The lack of correlation between rim fraction and crystal size suggests that proportionate crystal growth (Eberl et al., 2002), rather than ripening (Nemchin et al., 2001), controlled the formation of zircon rims in this sample.

In summary, we emphasize that (i) correct sectioning (Fig. S2) and (ii) a sufficiently large zircon population (Figs. 4, 7) is a requirement for successful application of the melt-o-meter based on rim volume fractions. Furthermore, (iii) it may be difficult to determine correct rim fractions if zircons are not sub-idiomorphic or at least large fragments of the original idiomorphic crystals.

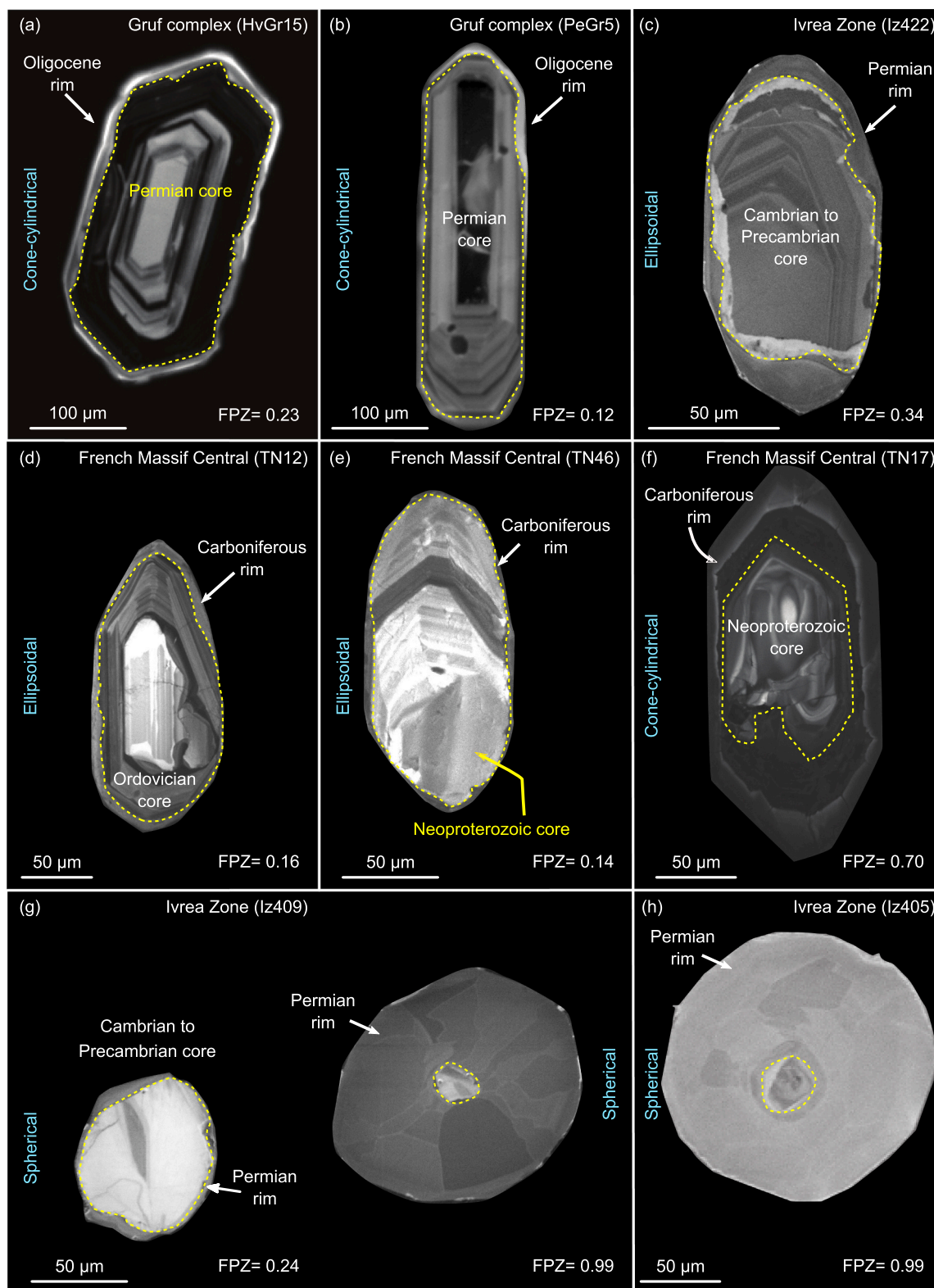


Fig. 3. Cathodoluminescence images of typical zircon grains from the migmatitic samples used in this study. Ages of cores and rims are U–Pb dating results in the corresponding studies (see text for references). Relative rim volume fraction FPZ ranging from 0.12 to 0.99. The geometrical model used to calculate the volumes (see Fig. 2) is indicated in blue. (For interpretation of the references to colour in this figure legend, the reader is referred to the web version of this article.)

4.2. Rim fraction populations

Our samples from natural migmatites reveal that the statistical distribution of zircon rim fractions strongly varies from one hand specimen to another (Fig. 4). Two extreme population types have been

identified (Fig. 4). In the first case, i.e. samples HvGr15, PeGr5, TN46, zircon rim fractions show narrow and nearly Gaussian distributions with full widths at half maximum (FWHM) of 0.10–0.12 (i.e. ± 0.05 – 0.06). Here, the relative zircon rim fraction is homogeneous across a sample, the average corresponding to the FPZ. As an example,

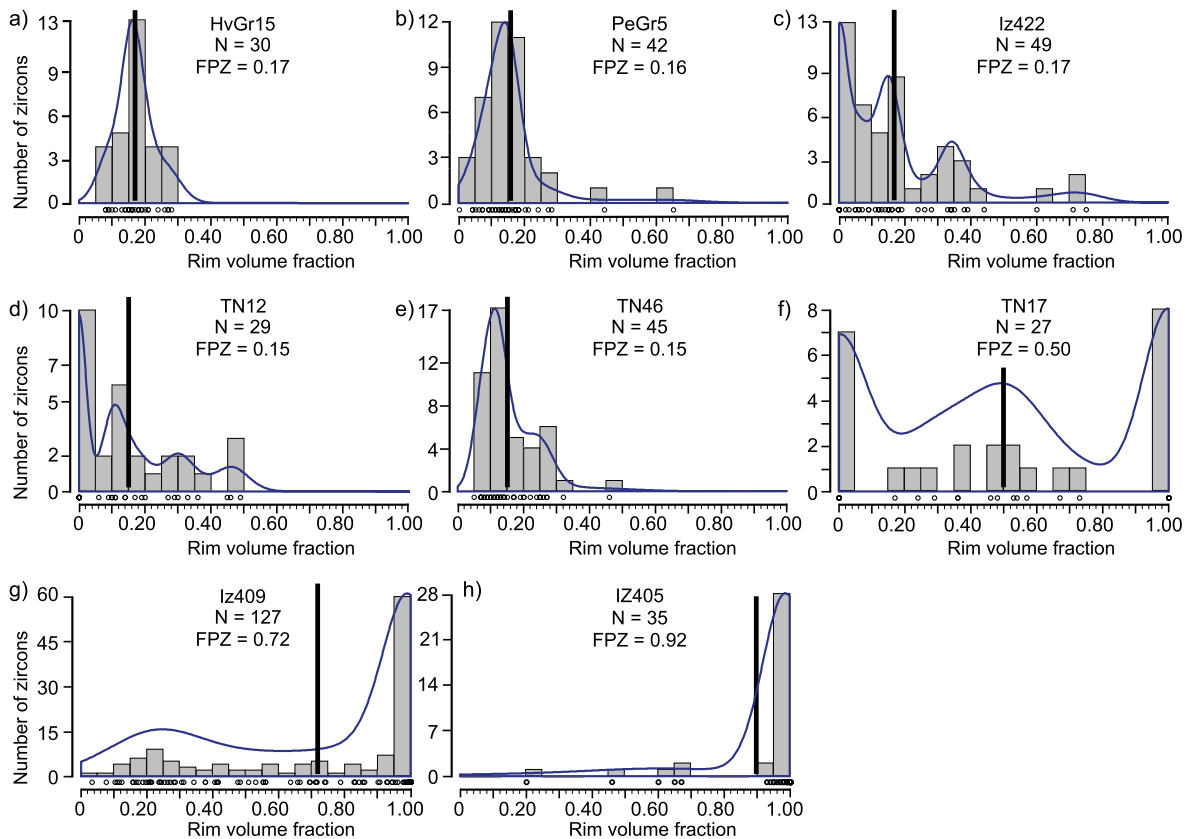


Fig. 4. Statistic representation of relative rim volume measurements of individual grains and their mean for the different worked samples. Three samples have narrow Gaussian populations (HvGr15, PeGr5, TN46). Two samples would have such populations but are skewed towards rimless zircons (Iz422, TN12), and two samples have almost bi-modal distributions with one peak towards rimless zircons. Iz405 has generally tiny cores, only few of them being larger. The 0.95–1.00 bins of TN17, Iz409 and Iz405 contain 8, 60, and 28 zircons without core, respectively. The complexity of distribution somewhat correlates with the heterogeneity of the sample (on the scale of the processed hand specimen; see text for details). Histogram and corresponding kernel-density estimates (KDE) of relative rim volume measurements.

the migmatitic fairly homogeneous orthogneiss HvGr15 yields a narrowly distributed rim fraction at 0.17 with a FWHM of 0.10 (Fig. 4a). The sample is dominated by a quartzo-feldspathic matrix with <15% biotite that itself is also homogeneously distributed. When accumulating measurements, the average FPZ becomes stable after only 5 measurements and varies <5% relative with the addition of any further measurements (Fig. 7a).

In the second case, i.e. samples Iz409 and TN17 (Fig. 4f, g), distributions of zircon rim fractions are heterogeneous, mostly bimodal. For example, in sample Iz409 a large number of grains have no or almost no core, but about ¼ of all grains show variable rim fractions averaging at ca. 0.25. The FPZ of 0.72, calculated averaging the rim fractions of all grains, corresponds to a low-frequency part of the statistical distribution (Fig. 4g). This sample is a migmatitic metapelite formed at 825 °C and 8 kbar with a characteristic heterogeneous texture and mineral distribution. It is not a surprise that macroscopically heterogeneous samples yield a heterogeneous zircon population. In biotite-rich, quartz-poor domains, shield effects of residual minerals (e.g. biotite or garnet) on their zircon inclusions would hinder direct contact between included zircons and anatectic melt, preventing zircon dissolution and re-precipitation (see also Yakymchuk and Brown, 2014). Watson et al. (1989) proposed that this shielding effect would preferentially affect small zircons over large ones, however, there is no significant variation of the average rim volume fraction with grain size in sample Iz409 (Fig. 6b). This is consistent with the rim-poor zircons, irrespective of their size, originating from unmolten (or less molten) domains rather than being included in single grains in the largely molten domain. In the quartzo-feldspathic matrix such shielding would

be much less important and the bimodal distribution of rim fractions likely reflects the sample heterogeneity in terms of largely molten quartz-rich vs. to a lesser degree molten biotite-rich domains. Here, ~70 measurements are required to obtain a stable average FPZ (Figs. 4, 7b) suggesting that heterogeneous samples require 50–100 individual measurements for obtaining a representative statistically robust FPZ.

Intermediate cases are represented by samples Iz422 and TN12, where the rim fraction distribution is skewed towards 0 (Fig. 4c, d). We suspect that again, the low rim fraction population represents zircons included within a single not molten mineral.

In any case, insofar bulk composition and Zr concentrations are also representative of the heterogeneous distribution of melt-rich and melt-poor domains, the calculated melt fractions for a given P-T condition satisfy the conditions for Eq. (3). Therefore, the average zircon rim fraction (e.g. 0.72 of Iz409) should represent the (average) FPZ at the sample scale and can be used to calculate an average F_{melt} . Nevertheless, the sharper the rim-fraction distribution, the more meaningful the average and the more straightforward the interpretation. It is hence in the best interest to take homogenous samples where ever possible.

4.3. Uncertainties on rim (FPZ) and melt fractions (F_{melt})

The uncertainty on average rim volume fractions should reflect the probability of the measured value to be representative of the true fraction of newly precipitated zircon FPZ at the sample scale. Using the examples above, the FPZ of HvGr15 is 0.17 ± 0.02 (2 S.E.) whereas it is 0.72 ± 0.06 (2 S.E.) for Iz409, which in both cases reflects well the variability of the running average (Fig. 7). Other uncertainties stem

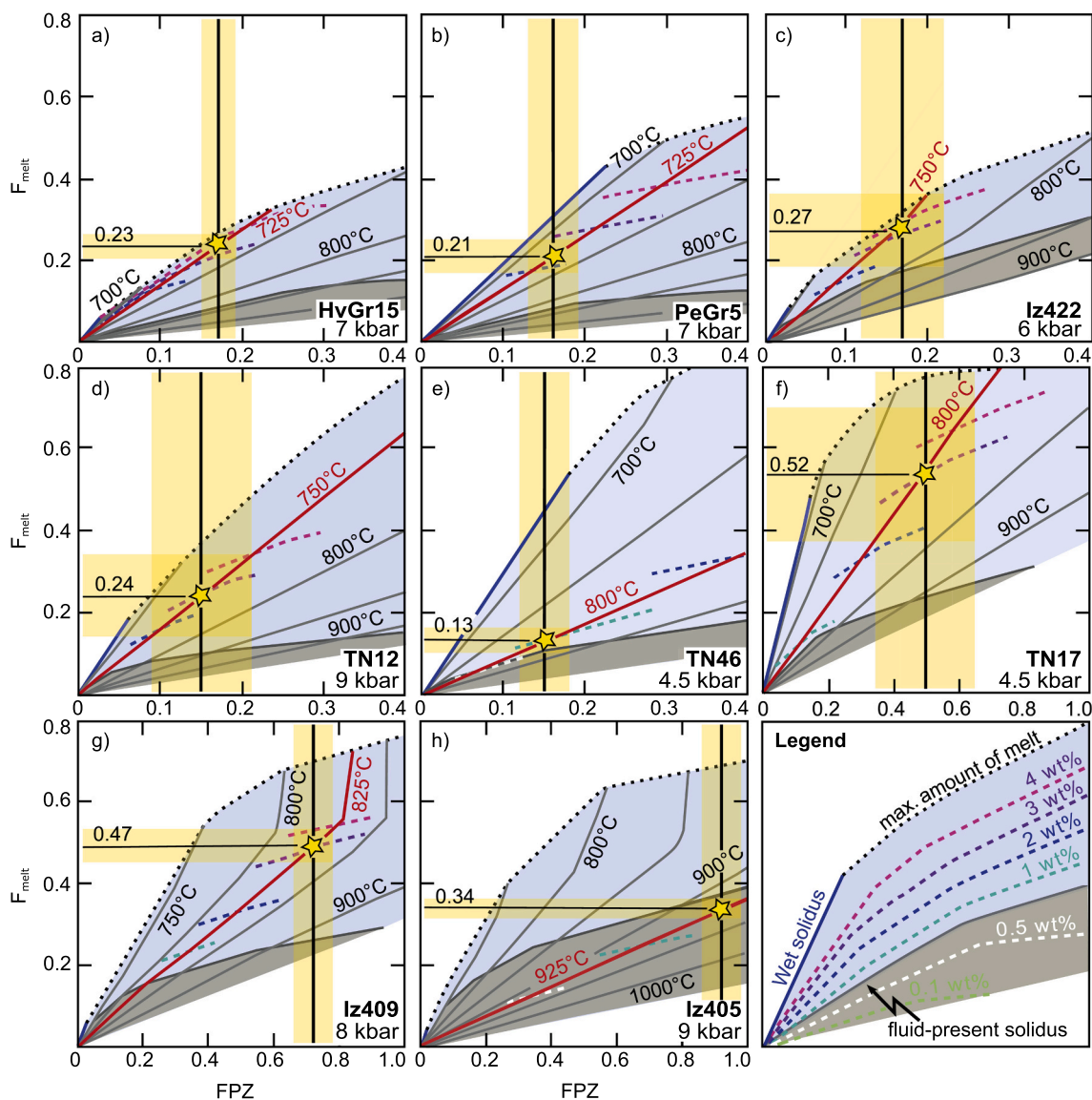


Fig. 5. Melt fraction (F_{melt}) as a function of fraction of newly precipitated zircon rims (FPZ) for the bulk composition of each of the eight worked migmatitic examples. F_{melt} for a given temperature and H_2O -content is computed using *Perple_X*. Pressure and temperature is known from the literature, F_{melt} is determined from the melt-o-meter (i.e. from FPZ) and hence, bulk H_2O -content at the time when the system closes for melt migration remains the unknown to be determined. The colored dashed lines indicate bulk H_2O -contents necessary to maintain the calculated amount of melt in a liquid state. The blue area depicts conditions where melting begins fluid-saturated, the gray area where it begins fluid-absent. The vertical black line represents the measured FPZ and the horizontal thin line the corresponding F_{melt} at peak temperature (red bold line). The yellow bands are the uncertainties on FPZ and F_{melt} . The dotted line gives the maximum amount of melt that can be formed in the given bulk composition at a given temperature (which corresponds to H_2O -saturated conditions). (For interpretation of the references to colour in this figure legend, the reader is referred to the web version of this article.)

from $[\text{Zr}]^{\text{sat}}$ and $[\text{Zr}]^{\text{bulk}}$, yet the uncertainty on $[\text{Zr}]^{\text{bulk}}$ (typically 5–10 ppm) is almost negligible relative to the other variables. As discussed earlier, the melt compositional parameter M does not vary much in metagranitic and metapelitic systems, such that the uncertainty on $[\text{Zr}]^{\text{sat}}$ mostly depends on temperature. The latter is case-specific but estimated to typically ± 10 to ± 30 °C. Note that there is no rigorous error propagation in any of the thermodynamic programs commonly used. The uncertainty on temperature propagates proportionally into F_{melt} , ± 10 °C leading to about $\pm 10\%$ relative on F_{melt} . Without considering the uncertainty in temperature, the propagated errors vary between 7 and 40% relative on F_{melt} , with a mean of 20% relative (Fig. 5 and Table 1). Larger zircon populations and an effort on geometrically reproducing rim shapes when calculating the 3D volumes clearly minimize uncertainties on the resulting F_{melt} .

4.4. Role of other Zr-bearing phases on the Zr budget and F_{melt}

Our method is applied and tested on granitoids *sensu lato* (meta-granites and -granodiorites) and on metapelites, in these the Zr budget during partial melting up to ~ 900 °C is almost completely controlled by zircon. At higher temperatures, and in particular in strongly residual granulites, other minerals may play a non-negligible role in the Zr budget. At $T > 900$ °C garnet may incorporate > 80 ppm Zr (Kohn et al., 2015) and rutile > 5000 ppm Zr (Ewing et al., 2013). Also, in mafic metamorphic rocks, amphibole and garnet can accommodate a significant fraction of the Zr budget because of their high modal abundance (Kohn et al., 2015). This precludes the use of the melt-o-meter in mafic systems. In principle these phases can be measured for Zr and corrections undertaken, however, the often strongly zoned nature of these phases would lead to substantially larger errors than estimated

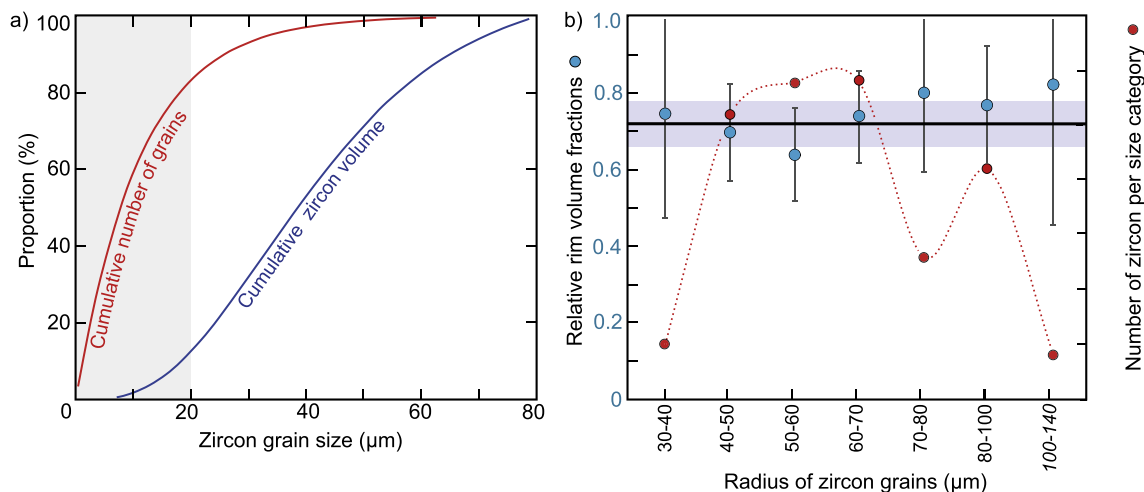


Fig. 6. (a) Diagram representing the CSD (crystal size distribution) and the associated cumulative zircon volume proportions (using a spherical volume), after Kawakami et al. (2013). The gray box highlights the contribution of grains < 20 μm. (b) Relative rim fractions (blue circles) and the number of zircon grains per size category (red circles) for Iz409 (8 kbar, 825 °C, $F_{\text{melt}} = 0.47$). The black bold line represents the average FPZ of 0.72 ± 0.06 (2 S.E.) obtained for this sample. (For interpretation of the references to colour in this figure legend, the reader is referred to the web version of this article.)

here.

Two of the tested samples (Iz405 and Iz409) have garnet in their mineral assemblages. Zr concentrations are reported for paragneisses close to Iz405 and Iz409 and garnets therein contain 50 and 20 ppm Zr, respectively (Bea and Montero, 1999; Bea et al., 2006). Applying a Zr-in-garnet correction, we obtain $F_{\text{melt}} = 0.46$ instead of 0.47 for Iz409 and 0.31 instead of 0.34 for Iz405. Iz405 contains also ~1 wt% rutile, for which, in adjacent metapelites, an average of 2800 ppm Zr is reported (Ewing et al., 2013). Correction for both garnet and rutile yield $F_{\text{melt}} = 0.27$. In summary, these corrections are minor and at the limit of the uncertainty on F_{melt} as determined by the melt-o-meter, however, more residual, garnet and rutile-rich samples would necessarily require such corrections.

5. Geological interpretation of melt fractions

In migmatitic rocks, melt segregation, extraction, migration, and depletion or accumulation are common processes (Sawyer, 1994).

During partial melting, commonly lasting for a few million years (Harris et al., 2000; Kelsey et al., 2008), any in- or out-flux of melt will modify the balance between residual zircon and the amount of Zr dissolved in the melt. However, as long as the migrating melts are zircon-saturated and temperature constant, the melt-flux does not interact with the undissolved zircon population. During heating, melt mobility is achieved when reaching the critical melt escape threshold, defined as the limit at which melt segregation occurs over large distances. At static or low strain conditions this threshold is thought to lie at 20–25 vol% in granitic systems (Vigneresse et al., 1996). Instead, under intense deformation the segregation threshold may be lowered to as little as ~7 vol% (Rosenberg and Handy, 2005).

Melt mobility during prograde heating may change F_{melt} and $[\text{Zr}]^{\text{bulk}}$, but will not be directly recorded by the melt-o-meter since this is accompanied by zircon dissolution. However, the volume of zircon rims ($V_{\text{zircon}}^{\text{rim}}$) to be crystallized upon cooling would be proportional to the net in- or out flux of Zr (and thus, melt) in the system. Therefore, the melt-o-meter based on FPZ informs on the conserved and crystallized

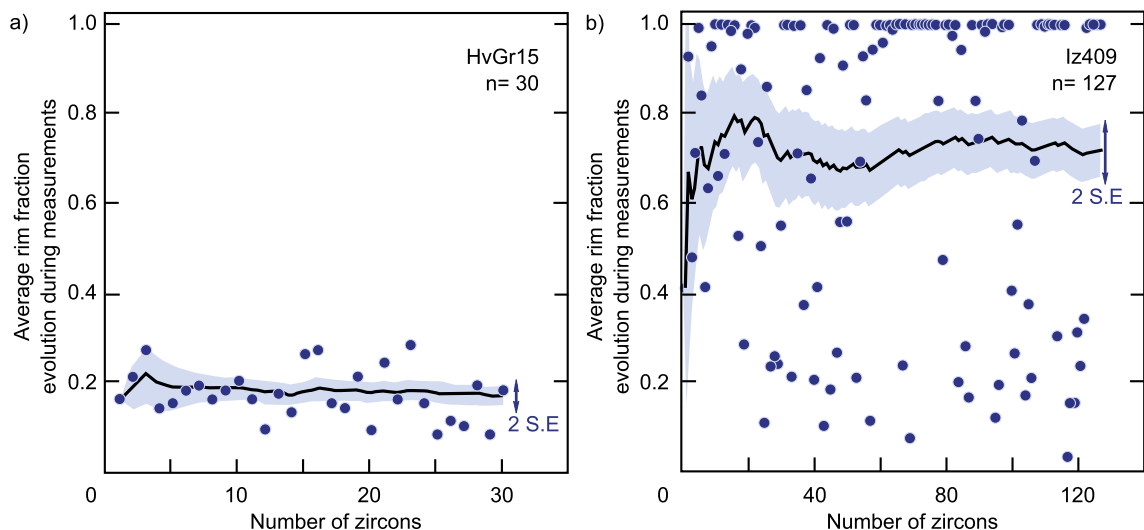


Fig. 7. Plots of measured relative rim volumes as a function of the number of measured grains, running average indicated as the thick black line, light blue area representing 2 σ (standard error, S.E). Statistical representation of relative rim volume measurements for (a) sample HvGr15 with a narrow, near Gaussian rim fraction distribution and (b) sample Iz409 with a heterogeneous rim fraction population (see Fig. 4). (For interpretation of the references to colour in this figure legend, the reader is referred to the web version of this article.)

amount of melt in a given rock volume. The only case, where interpretation becomes more complex is when significant amounts of melt crystallize during cooling while melt still migrates through the rock. In this case the zircon rim volume is still proportional to the frozen-in melt but not all of this melt has been a liquid when the system became closed to melt migration. This effect is expected to be of minor importance, because any significant in- and/or out flux of melt along a retrograde path is deemed unlikely (White and Powell, 2002).

Nevertheless, the melt-o-meter has several limits: It cannot inform on previous melt fluxes and the amount of melt that passed through the rock. As such, it does neither necessarily yield the maximum degree of melting that occurred in a given rock at metamorphic peak conditions nor does it directly provide information on the original rock fertility. The melt fraction F_{melt} obtained by our method is simply a snapshot of the melt fraction present at the time where the rock volume became a closed system in terms of melt mobility.

On the other hand, our melt-o-meter can be used as a first-order approximation to discuss the physical state of e.g. a leucosome at peak condition and melt mobility in migmatitic systems, the latter strongly depending on melt fraction (e.g. Sawyer, 1994; Vigneresse et al., 1996).

5.1. Near-solidus melting

Our migmatitic samples from peak temperatures of 700–750 °C (HvGr15, PeGr5 and TN12) yield F_{melt} of 0.21–0.24, show little or no evidence for *syn*-migmatitic deformation (e.g. dilatant sinks, shear bands) and are (geochemically) not considerably melt depleted. This suggests that these rocks remained nearly closed in terms of melt mobility at the hand specimen scale, F_{melt} is then an approximation of the maximum melt fraction produced during anatexis. In Iz422, formed at 750 °C, the melt-o-meter yields a F_{melt} of 0.27 ± 0.08 i.e. higher than the degree of melting of <0.15 derived from the thermodynamic modelling of Redler et al. (2013). This suggests either an accumulation of melt in this sample or an underestimated H_2O -content by Redler et al. (2013). In fact, for closed-system melting to produce a melt fraction of 0.27 in this rock, 3.5 wt% H_2O are required (from our thermodynamic calculation), while Redler et al. (2013) used 1.3 wt%, consequently obtaining a lower melt fraction.

5.2. Melting at ≥ 800 °C

Contrasting the near solidus samples, the melt-o-meter indicates that in the samples at $T > 800$ °C, the melt escape threshold is likely reached and melt transfer at larger scale becomes feasible (Vigneresse et al., 1996). Sample TN46 formed at 800 °C, and the F_{melt} of 0.13 ± 0.03 calculated with our melt-o-meter is considerably lower than the melt fraction estimated from thermodynamic modelling, i.e. 0.25–0.40 (Barbey et al., 2015, Table 1). This suggests that either part of the anatectic melt has connected and escaped the system or that the amount of H_2O effectively present in the rock was much lower than the H_2O -content used in the thermodynamic modelling (1.5 wt%). Conversely, F_{melt} of 0.47 ± 0.04 and 0.52 ± 0.16 are calculated with our method for Iz409 and TN17, respectively, which are higher than the melt fractions of 0.10–0.30 and 0.15–0.40 predicted by the thermodynamic modelling of Redler et al. (2013) and Barbey et al. (2015) (Table 1). This implies that both samples were most likely affected by melt in-flux and accumulation, yet, it is still possible that the amount of H_2O -used in the thermodynamic modelling was underestimated.

At >900 °C, the production of considerable amounts of melt are expected during anatexis. Sample Iz405 formed at 925 °C, the F_{melt} estimated with our melt-o-meter is 0.34 ± 0.02 , whereas the melt fraction estimated by the thermodynamic modelling of Redler et al. (2013) is 0.30–0.50 (Table 1). Although both estimates overlap, melt mobility is expected to be efficient at these conditions and it appears unlikely that the system remained closed for melt.

5.3. Interpretation of calculated H_2O contents

The results of our melt-o-meter may be combined with thermodynamic calculations to estimate the amount of H_2O at the time when the system closed for melt mobility. For this purpose, temperature- $X_{\text{H}_2\text{O}}$ pseudosections were calculated using Perple_X (Connolly, 2005) and phase modes analyzed. Such calculated H_2O contents strictly correspond to the amount of H_2O necessary to maintain the determined quantity of (granitic) melt at the given temperature and pressure in the liquid state.

As discussed above, samples HvGr15, PeGr5 and TN12, formed at 725–750 °C, likely remained closed in terms of melt mobility. Muscovite in these slightly peraluminous samples is absent (HvGr15 and PeGr5) or present in a small amount (TN12). The estimated temperatures indicate that these samples were near the fluid-absent muscovite melting reaction (Chatterjee and Johannes, 1974). However, this reaction should produce a melt fraction of only 0.07–0.15 (e.g. Vielzeuf and Holloway, 1988; Villaros et al., 2018), which is lower than the F_{melt} calculated from our melt-o-meter (0.21–0.24). Consequently, the amount of melting at melt fractions below the melt escape threshold is likely controlled by the influx of fluid. This is consistent with H_2O -contents of 2.2–3.5 wt% (10–12 wt% H_2O in the melt) obtained by combining the melt-o-meter with thermodynamic calculations (Fig. 5), i.e. with H_2O -contents far in excess of what could be stored in hydrous minerals at melting conditions. In addition, textural observations show that fluid-absent melting of biotite has not yet begun (Chelle-Michou et al., 2017; Galli et al., 2013), in agreement with experiments showing that fluid-absent biotite melting commences only at 850–875 °C (Vielzeuf and Holloway, 1988).

On the other extreme, melting in the granulite facies sample Iz405 (estimated peak temperature of 925 °C) is attributed to fluid-absent biotite melting (Fig. 5h). The calculated bulk H_2O -content is ~ 1.4 wt%, F_{melt} results to 0.34 (Fig. 5h). The H_2O -concentration in the (now frozen) melt was hence $\sim 4 \pm 1$ wt%, consistent with the 2–3 wt% to be expected from fluid-absent mica melting during which the mica/melt ratio is roughly 0.5 (Vielzeuf and Holloway, 1988). This sample indicates that despite a likely melt escape, the combination of the melt-o-meter with thermodynamic modelling allows to reconstruct plausible H_2O -contents also at high grade melting conditions.

5.4. Rheological implications

The re-precipitated zircon melt-o-meter constitutes a tool to quantify the amount of melt frozen in migmatitic rocks at a hand specimen scale and, if applied to several samples, of a partially molten unit on a larger scale. The ability to quantify and map the fraction of melt present in migmatitic rocks at the time of crystallization is crucial to retrieve the strength and viscosity of a rock and consequently understand its rheology. The drop in strength observed at 7–10 vol% melt (Rosenberg and Handy, 2005) strongly impacts the deformational behavior of rocks and hence the bulk rheology of the crust and its response to buoyancy and differential stress (Unsworth et al., 2005; Labrousse et al., 2015). As commonly observed throughout migmatitic terranes (e.g. Sawyer, 2008), the distribution of melt and therefore of low viscosity zones is heterogeneous and strongly controlled by anisotropy (e.g. shear zones), local stress gradients and rheological contrasts in the original configuration of the crust (e.g. lithological contacts).

Similarly, heterogeneous distributions of melt-rich, low viscosity zones concentrated in high-porosity domains are observed in deformation experiments (Katz et al., 2006), as well as in thermo-mechanical simulation of melt-assisted deformation (Gerya et al., 2015). Instead, in granitic to gneissic terranes, it is difficult to identify the amount of melt present at a given time. Our melt-o-meter allows for quantification of the melt distribution within specific domains towards the end of the last melting event. Similarly, if linked to field observations and applied on a regional scale on different domains, our

approach may consent to identify former soft, melt-rich and strong, melt-depleted domains, their distribution, array, size and extension, ultimately leading to the rheological mapping of high-grade terranes.

6. Conclusions

This work provides a new tool to quantify the amount of melt frozen in a hand sample of felsic, zircon saturated rocks in migmatitic terranes. The method requires bulk rock analysis, zircon U–Pb dating by spatially resolved techniques and careful determination of zircon rim volume fractions based on image processing. The melt-to-meter is independent from thermodynamic modelling, but combination with thermodynamic calculations allows retrieving H₂O-contents and to approximate the extent of melt mobility in migmatitic rocks. Used in combination, the two methods may further provide insights about the fluid-present vs. fluid-absent nature of partial melting. The samples tested here indicate that at temperatures insufficient for fluid-absent melting, fluid-influx controls the amount of melt.

Supplementary data to this article can be found online at <https://doi.org/10.1016/j.chemgeo.2020.119755>.

Declaration of competing interest

The authors declare that they have no known competing financial interests or personal relationships that could have appeared to influence the work reported in this paper.

Acknowledgements

We are grateful to ETH Zürich, Switzerland, for grant ETH-3416-1 to AG and MWS, which financed this study. J.A.C. Connolly is acknowledged for his help to realize the thermodynamic-modelling. We thank E. B. Watson and an anonymous reviewer for their helpful reviews and suggestions, which clarified the paper.

References

- Barbey, P., Villaros, A., Marignac, C., Montel, J.-M., 2015. Multiphase melting, magma emplacement and P-T-time path in late-collisional context: the Velay example (Massif Central, France). *Bulletin de la Société Géologique de France* 186 (2–3), 93–116. <https://doi.org/10.2113/gssgfbull.186.2-3.93>.
- Bartoli, O., 2017. Phase equilibria modelling of residual migmatites and granulites: an evaluation of the melt-reintegration approach. *J. Metamorph. Geol.* 35. <https://doi.org/10.1111/jmg.12261>.
- Bea, F., Montero, P., 1999. Behavior of accessory phases and redistribution of Zr, REE, Y, Th, and U during metamorphism and partial melting of metapelites in the lower crust: an example from the Kinzigite Formation of Ivrea-Verbano, NW-Italy. *Geochim. Cosmochim. Acta* 63, 1133–1153. [https://doi.org/10.1016/S0016-7037\(98\)00292-0](https://doi.org/10.1016/S0016-7037(98)00292-0).
- Bea, F., Montero, P., Ortega, M., 2006. A LA-ICP-MS evaluation of Zr reservoirs in common crustal rocks: implications for Zr and Hf Geochemistry, and zircon-forming processes. *Can. Mineral.* 44, 693–714. <https://doi.org/10.2113/gscanmin.44.3.693>.
- Boehnke, P., Watson, E.B., Trail, D., Harrison, T.M., Schmitt, A.K., 2013. Zircon saturation re-visited. *Chem. Geol.* 354, 324–334. <https://doi.org/10.1016/j.chemgeo.2013.05.028>.
- Bogaerts, et al., December 2006. Phase Equilibria of the Lyngdal Granodiorite (Norway): Implications for the Origin of Metaluminous Ferroan Granitoids, 2006. *J. Petrol.* 47 (12), 2405–2431. <https://doi.org/10.1093/ptrology/egl049>.
- Brown, M., Averkin, Y.A., McLellan, E.L., Sawyer, E.W., 1995. Melt segregation in migmatites. *J. Geophys. Res. Solid Earth* 100, 15655–15679. <https://doi.org/10.1029/95JB00517>.
- Chatterjee, N.D., Johannes, W., 1974. Thermal stability and standard thermodynamic properties of synthetic 2-M₁-muscovite, KAl₂[AlSi₃O₁₀(OH)₂]. *Contrib. Mineral. Petrol.* 48, 89–114. <https://doi.org/10.1007/BF00418612>.
- Chelle-Michou, C., Laurent, O., Moya, J.-F., Block, S., Paquette, J.-L., Couzinié, S., Gardien, V., Vanderhaeghe, O., Villaros, A., Zeh, A., 2017. Pre-Cadomian to late Variscan odyssey of the eastern Massif Central, France: formation of the west European crust in a nutshell. *Gondwana Res.* 46, 170–190. <https://doi.org/10.1016/j.jgr.2017.02.010>.
- Connolly, J.A.D., 2005. Computation of phase equilibria by linear programming: a tool for geodynamic modeling and its application to subduction zone decarbonation. *Earth Planet. Sci. Lett.* 236, 524–541. <https://doi.org/10.1016/j.epsl.2005.04.033>.
- Eberl, D.D., Kile, D.E., Virts, V.A., 2002. On geological interpretations of crystal size distributions: constant vs. proportionate growth. *Am. Mineral.* 87 (8–9), 1235–1241.
- Ewing, T.A., Hermann, J., Rubatto, D., 2013. The robustness of Zr-in-rutile and Ti-in-zircon thermometers during high-temperature metamorphism (Ivrea-Verbano Zone, northern Italy). *Contrib. Mineral. Petrol.* 165, 757–779. <https://doi.org/10.1007/s00410-012-0834-5>.
- Galli, A., Le Bayon, B., Schmidt, M.W., Burg, J.-P., Reusser, E., Sergeev, S.A., Larionov, A., 2012. U-Pb zircon dating of the Gruf complex: disclosing the late Variscan granulite lower crust of Europe stranded in the Central Alps. *Contrib. Mineral. Petrol.* 163, 353–378. <https://doi.org/10.1007/s00410-011-0676-6>.
- Galli, A., Le Bayon, B., Schmidt, M.W., Burg, J.-P., Reusser, E., 2013. Tectonometamorphic history of the Gruf complex (Central Alps): exhumation of a granulite-migmatite complex with the Bergell pluton. *Swiss J. Geosci.* 106, 33–62. <https://doi.org/10.1007/s00015-013-0120-1>.
- Gardien, V., Lardeaux, J.-M., Ledru, P., Allemand, P., and Guillot, S., 1997. Metamorphism during late orogenic extension: insights from the French Variscan belt: Bulletin de la Société Géologique de France, t. 168, n°3, p. 271–286.
- Gerdes, A., Zeh, A., 2009. Zircon formation versus zircon alteration – new insights from combined U-Pb and Lu-Hf in-situ LA-ICP-MS analyses, and consequences for the interpretation of Archean zircon from the Central Zone of the Limpopo Belt. *Chem. Geol.* 261, 230–243. <https://doi.org/10.1016/j.chemgeo.2008.03.005>.
- Gerya, T.V., Stern, R.J., Baes, M., Sobolev, S.V., Whattam, S.A., 2015. Plate tectonics on the earth triggered by plume-induced subduction initiation. *Nature* 527, 221–225. <https://doi.org/10.1038/nature15752>.
- Harris, N., Vance, D., Ayres, M., 2000. From sediment to granite: timescales of anatexis in the upper crust. *Chem. Geol.* 162, 155–167. [https://doi.org/10.1016/S0009-2541\(99\)00121-7](https://doi.org/10.1016/S0009-2541(99)00121-7).
- Harrison, T.M., Watson, E.B., 1983. Kinetics of zircon dissolution and zirconium diffusion in granitic melts of variable water content. *Contrib. Mineral. Petrol.* 84, 66–72. <https://doi.org/10.1007/BF01132331>.
- Holland, T.J.B., Powell, R., 2011. An improved and externally-consistent thermodynamic dataset for phases of petrological interest, involving a new equation of state for solids. *J. Metamorph. Geol.* 29, 333–383.
- Holtzman, B.K., Groebner, N.J., Zimmerman, M.E., Ginsberg, S.B., Kohlstedt, D.L., 2003. Stress-driven melt segregation in partially molten rocks. *Geochem. Geophys. Geosyst.* 4 (5), 8607. <https://doi.org/10.1029/2001GC000258>.
- Katz, R.F., Spiegelman, M., Holtzman, B., 2006. The dynamics of melt and shear localization in partially molten aggregates. *Nature* 442, 676–679. <https://doi.org/10.1038/nature05039>.
- Kawakami, T., Yamaguchi, I., Miyake, A., Shibata, T., Maki, K., Yokoyama, T.D., Hirata, T., 2013. Behavior of zircon in the upper-amphibolite to granulite facies schist/migmatite transition, Ryoke metamorphic belt, SW Japan: constraints from the melt inclusions in zircon. *Contrib. Mineral. Petrol.* 165, 575–591. <https://doi.org/10.1007/s00410-012-0824-7>.
- Kelsey, D.E., Clark, C., Hand, M., 2008. Thermobarometric modelling of zircon and monazite growth in melt-bearing systems: examples using model metapelitic and metapsammite granulites. *J. Metamorph. Geol.* 26, 199–212. <https://doi.org/10.1111/j.1525-1314.2007.00757.x>.
- Klimm, K., Holtz, F., Johannes, W., King, P.L., 2003. Fractionation of metaluminous A-type granites: an experimental study of the Wangrah Suite, Lachlan Fold Belt, Australia. *Precambrian Res.* 124, 327–341. [https://doi.org/10.1016/S0301-9268\(03\)00092-5](https://doi.org/10.1016/S0301-9268(03)00092-5).
- Kohn, M.J., Corrie, S.L., Markley, C., 2015. The fall and rise of metamorphic zircon. *Am. Mineral.* 100 (4), 897–908. <https://doi.org/10.2138/am-2015-5064>.
- Kunz, E.B., Regis, D., Engi, M., 2018. Zircon ages in granulite facies rocks: decoupling from geochemistry above 850 °C? *Contrib. Mineral. Petrol.* 173, 26. <https://doi.org/10.1007/s00410-018-1454-5>.
- Labrousse, L., Duret, T., Gerya, T., 2015. H₂O-fluid saturated melting of subducted continental crust facilitates exhumation of ultrahigh-pressure rocks in continental crust subduction zones. *Earth Planet. Sci. Lett.* 428, 151–161. <https://doi.org/10.1016/j.epsl.2015.06.016>.
- Mayne, M.J., Moya, J.-F., Stevens, G., Kaislaniemi, L., 2016. Rcrust: a tool for calculating path-dependent open system processes and application to melt loss. *J. Metamorph. Geol.* 34, 663–682. <https://doi.org/10.1111/jmg.12199>.
- Montel, J.-M., Vielzeuf, D., 1997. Partial melting of metagreywackes, Part II. Compositions of minerals and melts. *Contrib. Mineral. Petrol.* 128, 176–196. <https://doi.org/10.1007/s0041000050302>.
- Nemchin, A.A., Giannini, L.M., Bodorkos, S., Oliver, N.H.S., 2001. Otswald ripening as a possible mechanism for zircon overgrowth formation during anatexis: theoretical constraints, a numerical model, and its application to pelitic migmatites of the Tickalara metamorphics, northwestern Australia. *Geochim. Cosmochim. Acta* 65, 2771–2788. [https://doi.org/10.1016/S0016-7037\(01\)00622-6](https://doi.org/10.1016/S0016-7037(01)00622-6).
- Patiño Douce, A.E., Beard, J.S., 1996. Effects of P, f(O₂) and Mg/Fe ratio on Dehydration Melting of Model Metagreywackes. *J. Petrol.* 37, 999–1024.
- Patiño Douce, A.E., Harris, N., 1998. Experimental Constraints on Himalayan Anatexis. *J. Petrol.* 39, 689–710. <https://doi.org/10.1093/ptro/39.4.689>.
- Redler, C., White, R.W., Johnson, T.E., 2013. Migmatites in the Ivrea Zone (NW Italy): constraints on partial melting and melt loss in metasedimentary rocks from Val Strona di Omega. *Lithos* 175–176, 40–53. <https://doi.org/10.1016/j.lithos.2013.04.019>.
- Rosenberg, C.L., Handy, M.R., 2005. Experimental deformation of partially melted granite revisited: implications for the continental crust. *J. Metamorph. Geol.* 23, 19–28. <https://doi.org/10.1111/j.1525-1314.2005.00555.x>.
- Rudnick, R.L., Gao, S., 2003. Composition of the Continental Crust: Treatise on Geochemistry. 3. pp. 1–64. <https://doi.org/10.1016/B0-08-043751-6/03016-4>.
- Rutter, E.H., Neumann, D.H., 1995. Experimental deformation of partially molten Westerly granite under fluid-absent conditions, with implications for the extraction of granitic magmas. *J. Geophys. Res.* 100, 15697–15715. <https://doi.org/10.1029/>

- 94JB03388.
- Sawyer, E.W., 1987. The role of partial melting and fractional crystallization in determining discordant migmatite leucosome compositions. *J. Petrol.* 28, 445–473. <https://doi.org/10.1093/petrology/28.3.445>.
- Sawyer, E.W., 1994. Melt segregation in the continental crust. *Geology* 22, 1019–1022. [https://doi.org/10.1130/0091-7613\(1994\)022<1019:MSITCC>2.3.CO;2](https://doi.org/10.1130/0091-7613(1994)022<1019:MSITCC>2.3.CO;2).
- Sawyer, E.W., 2008. *Atlas of Migmatites: The Canadian Mineralogist, Special Publication 9*. NRC Research Press, Ottawa, Ontario, Canada, pp. 371.
- Singh, J., Johannes, W., 1996. Dehydration melting of tonalities. Part II. Composition of melts and solids. *Contrib. Mineral. Petrol.* 125, 26–44. <https://doi.org/10.1007/s004100050204>.
- Stevens, G., 1995. *Compositional controls on partial melting in high-grade metapelites; a petrological and experimental study* (unpublished). PhD thesis. Univ Manchester.
- Stevens, G., Villaros, A., Moyen, J.-F., 2007. Selective peritectic garnet entrainment as the origin of geochemical diversity in S-type granites. *Geology* 35, 9–12. <https://doi.org/10.1130/G22959A.1>.
- Unsworth, M.J., Jones, A.G., Wei, W., Marquis, G., Gokarn, S.G., Spratt, J.E., The INDEPTH-MT team, 2005. *Nature* 438, 78–81. <https://doi.org/10.1038/nature04154>.
- Vanderhaeghe, O., 2009. Migmatites, granites and orogeny: flow modes of partially-molten rocks and magmas associated with melt/solid segregation in orogenic belts. *Tectonophysics* 477, 119–134. <https://doi.org/10.1016/j.tecto.2009.06.021>.
- Vielzeuf, D., Holloway, J.R., 1988. Experimental determination of the fluid-absent melting relations in the pelitic system. *Contrib. Mineral. Petrol.* 98, 257–276.
- Vigneresse, J.-L., Barbey, P., Cuney, M., 1996. Rheological transitions during partial melting and crystallization with application to felsic magma segregation and transfer. *J. Petrol.* 37, 1579–1600. <https://doi.org/10.1093/petrology/37.6.1579>.
- Villaros, A., Stevens, G., Moyen, J.-F., Buick, I.S., 2009. The trace element compositions of S-type granites: evidence for disequilibrium melting and accessory phase entrainment in the source. *Contrib. Mineral. Petrol.* 158, 543–561. <https://doi.org/10.1007/s00410-009-0396-3>.
- Villaros, A., Laurent, O., Couzinié, S., Moyen, J.-F., and Mintrone, M., 2018. Plutons and domes: the consequences of anatectic magma extraction-example from the south-eastern French Massif Central: *Int. J. Earth Sci.* v. 107, p. 2819–2842, doi:<https://doi.org/10.1007/s00531-018-1630-x>.
- Villaseca, C., Belousova, E., Orejana, D., Castiñeiras, P., Pérez-Soba, C., 2011. Presence of Palaeoproterozoic and Archean components in the granulite-facies rocks of central Iberia: the Hf isotopic evidence. *Precambrian Res.* 187, 143–154. <https://doi.org/10.1016/j.precamres.2011.03.001>.
- Watson, E.B., 1996. Dissolution, growth and survival of zircons during crustal fusion; kinetic principals, geological models and implications for isotopic inheritance. *Trans. R. Soc. Edinb. Earth Sci.* 87, 43–56. <https://doi.org/10.1017/S0263593300006465>.
- Watson, E.B., Harrison, T.M., 1983. Zircon saturation revisited: temperature and composition effects in a variety of crustal magma types. *Earth Planet. Sci. Lett.* 64, 295–304. [https://doi.org/10.1016/0012-821X\(83\)90211-X](https://doi.org/10.1016/0012-821X(83)90211-X).
- Watson, E.B., Vicenzi, E.P., Rapp, R.P., 1989. Inclusion/host relations involving accessory minerals in high-grade metamorphic and anatectic rocks. *Contrib. Mineral. Petrol.* 101, 220–231.
- Weinberg, R.F., Hasalová, P., 2015. Water-fluxed melting of the continental crust: a review. *Lithos* 212–215, 158–188. <https://doi.org/10.1016/j.lithos.2014.08.021>.
- White, R.W., Powell, R., 2002. Melt loss and the preservation of granulite facies mineral assemblages. *J. Metamorph. Geol.* 20, 621–632. <https://doi.org/10.1046/j.1525-1314.2002.00206.20.7.x>.
- White, R.W., Powell, R., Holland, J.B., 2001. Calculation of partial melting equilibria in the system Na₂O-CaO-K₂O-FeO-MgO-Al₂O₃-SiO₂-H₂O (NCKFMASH). *J. Metamorph. Geol.* 19, 139–153. <https://doi.org/10.1046/j.0263-4929.2000.00303.x>.
- White, R.W., Powell, R., Halpin, J.A., 2004. Spatially-focussed melt formation in aluminous metapelites from Broken Hill, Australia. *J. Metamorph. Geol.* 22, 825–845. <https://doi.org/10.1111/j.1525-1314.2004.00553.x>.
- Yakymchuk, C., Brown, M., 2014. Behaviour of zircon and monazite during crustal melting. *J. Geol. Soc.* 171, 465–479. <https://doi.org/10.1144/jgs2013-115>.